Development and Application of Acousto-Optic Background Correction for Inductively Coupled Plasma Atomic Emission Spectrometry

HEATHER M. MILLER, THOMAS M. SPUDICH, and JON W. CARNAHAN*

Department of Chemistry and Biochemistry, Northern Illinois University, DeKalb, Illinois 60115 (H.M.M., J.W.C.); and School of Science, Penn State Erie, The Behrend College, Erie, Pennsylvania 16563 (T.M.S.)

In two configurations, a solid-state acousto-optic (AO) deflector or modulator is mounted in a 0.5 m monochromator for background correction with inductively coupled plasma atomic emission spectrometry (ICP-AES). A fused silica acousto-optic modulator (AOM) is used in the ultraviolet (UV) spectral region applications while a glass AO deflector (AOD) is used for the visible (VIS) region. The system provides rapid sequential observation of adjacent on- and off-line wavelengths for background correction. Seventeen elements are examined using pneumatic nebulization (PN) and electrothermal vaporization (ETV) sample introduction. Calibration plots were obtained with each sample introduction technique. Potable water and vitamin tablets were analyzed. Flame atomic absorption (FAA) was used to verify the accuracy of the AO background correction system.

Index Headings: **Acousto-optic deflector; Acousto-optic modulator; Background correction; Inductively coupled plasma; Electrothermal vaporization; Flame atomic absorption.**

INTRODUCTION

Inductively coupled plasma atomic emission spectrometry (ICP-AES) is a robust and versatile source for trace-metals analysis. This technique is used for the analysis of a wide variety of samples. A sampling of recent publications illustrate ICP-AES being used for the determination of metals in drinking water,[1] food,[2–4] soils,[5,6] biological materials,[7,8] and many other samples.

Inherent plasma flicker dictates that best results are obtained when it is possible to correct for ''baseline'' or ''background'' instabilities. Various background correction methods have been examined. Charge-coupled and injection devices (CCD and CID) are becoming the dominant detectors for ICP-AES. While excellent for background correction, these detectors have moderately high costs, require system complexity, and produce large data files that require considerable manipulation time. When fewer elements are determined with high throughput, ICP spectrometers with photomultiplier tube (PMT) detectors are still widely in use. PMTs offer high efficiency in a single unit detector and are less expensive than CCDs and CIDs.

For background correction using PMTs, techniques often involve the movement of devices such as refractor plates, choppers, and gratings. Since these methods involve moving objects, there are inertia-based limitations that limit their effectiveness and speed. Acousto-optic devices offer a solid-state alternative for background correction. Acousto-optic deflectors and modulators have been used for many years in applications such as laser beam steering. The detailed theory of AODs and AOMs has been presented elsewhere.[9–12] In short, radiation enters and travels through a transparent AO material. A piezo-electric transducer, driven at a frequency in the tens to hundreds of megahertz range, is used to launch compression waves in the AO medium. The wave travels at a near-acoustic velocity in a direction nearly perpendicular to the path of the radiation traversing the AO medium. As the radiation interacts with the acoustic waves inside the AO medium, the radiation undergoes diffraction. The deflection angle is proportional to the applied frequency. By mounting the AO device in the light path within a monochromator, the diffracted light can be directed on and off the exit slit. This arrangement facilitates monitoring of analytical atomic emission signals and the ''off-line'' background in quick succession by modulating the applied AO frequency. This method has been successfully employed and characterized with hollow cathode lamps (HCL) and microwave-induced plasmas (MIP) in our research group.[13]

While incorporating the AOD background correction scheme with MIP-AES, pneumatic nebulization and electrothermal vaporization (ETV) were used as sample introduction methods. Pneumatic nebulization typically leads to poorer detection limits than ETV. This is due to the low transport efficiency to the plasma and the poor efficiency of converting aqueous samples into aerosol. The use of ETV offers the advantages of smaller sample volume requirements, higher transport efficiencies, and lower detection limits.[14] A disadvantage of ETV methods is the introduction of background-signal fluctuations by the gas expansion during the analyte vaporization cycle. The increase in temperature and subsequent gas expansion causes pressure fluctuations, which change the intensity of the background emission. These fluctuations are significant and can degrade analytical performance. Therefore, background correction is needed to compensate for the background shifts.[13,15]

In this article, the AO background correction system is characterized with ICP-AES from 200 to 700 nm using two AO devices. Seventeen elements are analyzed using a fused silica AOM and a glass AOD. Characterization and system operation is detailed. Calibration plots for these elements are presented using both PN and ETV sample introduction. Finally, tap water and vitamin tablets are analyzed for the concentrations of six elements. Flame atomic absorption spectrometry is used to compare the results obtained with the AO background correction ICP-AES system.

Received 24 August 2002; accepted 31 January 2003.
* Author to whom correspondence should be sent.

0003-7028/03/5706-0703$2.00/0

TABLE I. Perkin-Elmer model 3110 atomic absorption spectrometer operating conditions.[a]

Element	Wavelength (nm)	HCL current (mA)	Slit (nm)	Gas flow rates (mL/min)		Range of Std. Conc. (μg/mL)
				Acetylene	Air	
Ca	422.7	25	0.7	2.5	4.0	1–5
Cu	324.8	20	0.7	2.5	4.0	1–3
Fe	248.3	25	0.2	2.5	4.0	0.5–2
Mg	285.3	25	0.7	2.5	4.0	1–5
Zn	213.9	15	0.7	2.5	4.0	1–5

[a] Sample uptake rate: 5 mL/min, data acquisition: five 5-s readings for all samples and standards.

EXPERIMENTAL METHODS

Instrumentation. For the atomic absorption experiments, a Perkin-Elmer model 3110 atomic absorption spectrometer with an air–acetylene flame was utilized. An iron hollow cathode lamp was obtained from Fisher Scientific Company (Fairlawn, NJ). Copper, zinc, and calcium/magnesium lamps were obtained from Westinghouse. Table I lists specific conditions for each element analyzed.

For all ICP-AES measurements, the plasma portion of a Varian Liberty Series II axial ICP spectrometer was used. Table II lists 23 elemental emission wavelengths for the 17 elements studied. The other information in the table will be discussed later in the text.

An acousto-optic deflector or modulator (model ADM-40 or ASM-704B0, respectively, IntraAction Corporation, Inc., Bellwood, IL) was mounted in the light path of a modified 0.5-m-focal-length Czerny–Turner scanning monochromator (model 82-516 Jarrell Ash, Co., Waltham, MA). The placement of the AO was 2.0 cm behind the entrance slit. A schematic diagram of the acousto-optic and monochromator setup can be seen elsewhere.[13]

The AOD in this study has a manufacturer-specified visible wavelength range of 440 to 700 nm and is constructed of dense flint glass. A manufacturer-installed 2 × 20 mm rectangular optical aperture masked with a 1.3-mm-diameter copper aperture is utilized in all experiments with the glass AOD. The AOD driver (model DE-40 VCO deflector driver, IntraAction Corporation, Inc.) has a center frequency of 40 MHz, a range of 27 to 54 MHz, and a maximum RF power of 4 W.

The AOM has a manufacturer-specified UV wavelength range of 300 to 400 nm, is constructed of UV-grade fused silica, and has a manufacturer-installed 2 × 20 mm optical aperture. Masks with circular diameters of 1.0, 1.2, 1.5, 1.8, 2.0, 2.5, and 3.0 mm were interchangeably mounted on the AOM. The AOM driver (model DE-705M VCO deflector driver, IntraAction Corporation, Inc.) has a maximum RF power of 5 W, a center frequency of 70 MHz, and a frequency range of 50 to 90 MHz. A frequency counter is used to monitor the applied acoustic frequency to the AOD or AOM (model 5245 L electronic counter, Hewlett Packard).

The plasma was focused onto the 20 μm entrance slit of the monochromator using a 12.5-cm-focal-length lens at an object distance of 56 cm. The radiation intensity from the ICP was recorded after passing through the 15 μm exit slit using a 1P28A PMT (Hamamatsu, Toyooka Vill, Japan) maintained with a −1000 V bias with a high-voltage power supply (model 246, Keithley Instruments, Cleveland, OH). The PMT output current was converted to a voltage, amplified, and filtered using a system constructed at Northern Illinois University. The output voltage was directed to a SCB-68 connector and an AT-MIO-16XE-10 data acquisition board (National Instruments, Austin, TX) installed in a PC. LabView version 6i (National Instruments, Austin, TX) was used to write data acquisition/manipulation software. This code allowed one to acquire the PMT signal as a function of time and perform acousto-optic frequency modulation. The measured data was saved as an ASCII text file for further analysis.

TABLE II. Frequency modulation parameters.

Element	Zero-order wavelength (nm)	Acoustic frequency (MHz)		First-order wavelength position (nm)	
		On-line (analytical)	Off-line (background)	On-line (analytical)	Off-line (background)
Ag	328.068	68	108	329.2	329.7
Ba	233.527	68	108	234.0	234.4
Be	234.861	68	108	235.4	235.8
Ca	393.366	68	28	394.5	393.9
Ca	422.673	36	52	423.8	424.2
Cd	214.438	68	108	215.0	215.4
Co	228.616	68	28	229.2	228.6
Cr	267.716	68	108	268.3	268.7
Cr	427.291	36	20	428.0	427.4
Cr	428.972	36	24	429.8	429.5
Cu	324.754	68	108	325.5	325.9
Eu	381.967	68	100	382.8	383.3
Fe	238.204	68	52	238.8	238.6
Li	670.776	36	52	671.9	672.3
Mg	280.270	68	108	280.9	281.3
Mn	257.610	68	108	258.3	258.7
Mn	403.076	36	56	403.9	404.4
Na	588.995	36	52	590.6	591.0
Na	589.592	36	56	591.1	591.6
Pb	220.353	68	100	220.9	221.1
Sc	361.384	68	108	362.2	362.8
Sc	437.446	36	52	438.6	439.0
Zn	213.856	68	108	214.4	214.8

The electrothermal vaporizer used in this study was described in a previous publication.[15] A Varian Model 63 atomizer (Varian Techtron, Melbourne, Australia) that uses carbon cup (Part No. 99-200335-00) electrothermal vaporization is utilized. The 15 μL samples were introduced into the carbon cup using a Pipetman adjustable pipet (Model K-62-14871, Gilson, France). For samples that required a matrix modifier, 5 μL of 10500 μg/mL $Mg(NO_3)_2$ was injected into the cup using a 5 μL Eppendorf pipet (Model 3130, Germany). An argon flow rate of 1 L/min was used to carry the vaporized sample to the plasma.

Standards and Samples. Stock solutions were prepared by dissolving reagent-grade salts in 1% (v/v) nitric acid (Fisher Scientific Company, Fairlawn, NJ). Solutions of 100 μg/mL of Ag, Ca, Cd, Co, Cr, Cu, Eu, Fe, Li, Mn, Na, Pb, Sc, and Zn were prepared in this manner. Salts obtained from J.T. Baker Chemical Company (Phillipsburg, NJ) were $Ca(NO_3)_2$, $Cu(NO_3)_2 \cdot 3H_2O$, and $CdCl_2 \cdot 2\ ½\ H_2O$. Salts obtained from Fisher Scientific Company (Fairlawn, NJ) were LiCl, K_2CrO_4, $Zn(NO_3)_2 \cdot 6\ H_2O$, $Pb(NO_3)_2$, $AgNO_3$, and $Fe(NO_3)_3 \cdot 9\ H_2O$. Manganese sulfate monohydrate ($MnSO_4 \cdot H_2O$) was obtained from

Mallinckrodt Chemical Works (St. Louis, MO), $NaNO_3$ from Merck & Company, Inc. (Rahway, NJ), Eu_2O_3 from Acros (Geel, Belgium), and $Co(NO_3)_3$ from ICN Biomedicals Inc. (Aurora, OH). For 100 μg/mL solutions of Ba, Be, and Mg, commercially available ICP standards (Inorganic Ventures, Inc., Lakewood, NJ) were diluted in 1% (v/v) nitric acid. Scandium solutions were made from a standard solution (Spex CertiPrep, Mituchen, NJ) as well. All calibration solutions were prepared from the 100 μg/mL standards.

For the vitamin samples, a tablet of Advanced Formula Centrum (Whitehall-Robins Healthcare, Madison, NJ) was dissolved in approximately 50 mL of deionized water and sonicated (model 08849-00 ultrasonic cleaner, Cole-Parmer, Chicago, IL) for 10 min. After dissolution of the tablet was complete, the sample was vacuum filtered using a gouch crucible to remove any undissolved material. The filtrate was diluted to 100 mL in a volumetric flask. This procedure was followed for 5 tablets total. Taking aliquots from these stock vitamin solutions and diluting with 1% (v/v) nitric acid created all samples analyzed. Tap water samples were collected from a Kirkland, IL, farmhouse, acidified with concentrated nitric acid to pH < 2, and sealed in a plastic bottle. The tap was left running for five minutes before sample collection occurred. Five aliquots from the acidified tap water were taken.

RESULTS AND DISCUSSION

Optimization. Having a system similar to that previously used, it was possible to utilize parameters similar to those found in the visible glass AOD optimization.[13] Therefore, the reader is referred to that reference for additional details. This section deals primarily with optimization of the ultraviolet fused silica AOM, with additional notes where necessary regarding the glass AOD.

Acousto-Optic Masking . In our previous work with the microwave-induced plasma atomic emission source, it was found that line widths were significantly increased by reflections within the AOD.[13] Detailed studies with a range of masks indicated that a 1.3-mm-circular-diameter aperture at the face of the AOD provided the best compromise between maximum light throughput, AOD diffraction efficiencies, and reflection-induced peak broadening. Experiments similar to those cited in Ref. 13 were carried out with the fused silica AOM. The AOM was mounted in the monochromator in the same manner as the glass AOD.

Spectra were recorded for the Cu ICP emission lines at 324.754 and 327.396 nm. The Cu concentration was 100 μg/mL. In Fig. 1A, the spectrum for Cu when no AO is present in the light path is shown. Symmetric emission peaks are seen and the full width at half-maximum (FWHM) of the 324.7 nm Cu line is 0.16 nm. The AOM was mounted in the monochromator and rotated until the maximum intensity first-order AOM diffracted peaks were observed. Figure 1B shows the copper spectrum with the AOM in the light path with the original 2 × 20 mm aperture, but no power applied to the AOM driver. The zero-order peaks (zero order with respect to AOM diffraction, first-order grating diffraction) exhibit ''sloping shoulders'' to the high wavelength side. Using an AOM driver frequency of 74 MHz and a driver power of

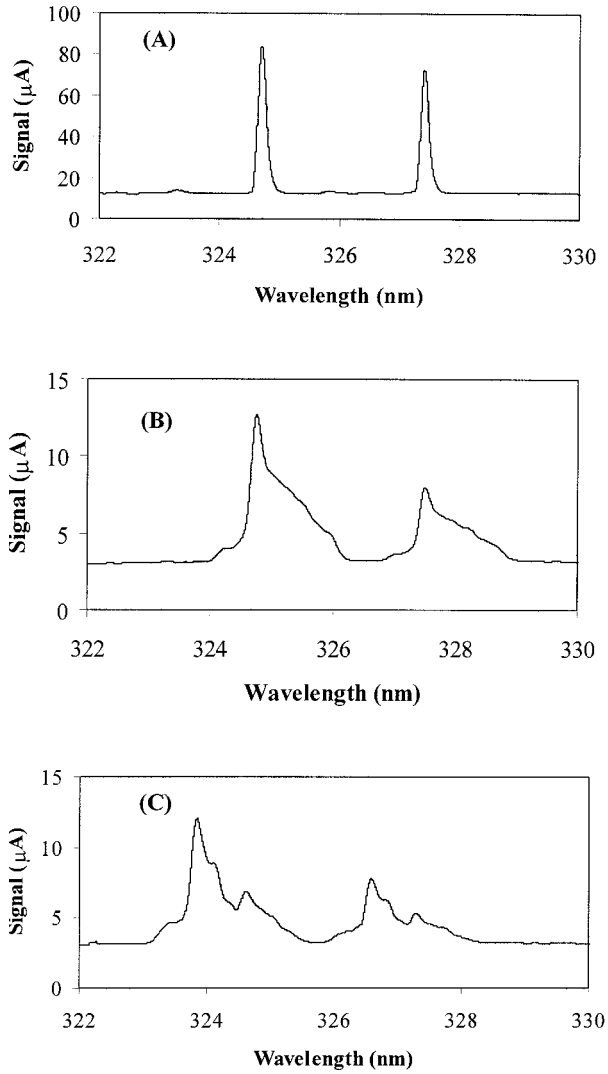

FIG. 1. Cu emission spectral effects of the AOM with a 2 × 20 mm rectangular aperture. (**A**) No AOM present in the light path of the monochromator and driver power off. (**B**) AOM in the light path and the driver power off. (**C**) AOM in the light path, driver power at 5 W, and frequency of 74 MHz.

5 W, acousto-optic diffraction of the copper emission occurs; results are shown in Fig. 1C. The first-order AO diffracted peak for 324.7 nm Cu is seen at the monochromator calibrated position of 325.6 nm. A similar pattern is seen with the less intense 327.4 nm Cu line with the first-order peak present at 328.3 nm.

As shown in the spectra obtained with no masking of the original rectangular aperture, it is difficult to observe first-order AO diffraction. The primary problem is due to reflections within the AOM. This situation creates the peak shoulders than are seen in Figs. 1B and 1C. This phenomenon has also been observed with the glass AOD.[13] Therefore, circular masks of varying diameter were applied to the AOM to minimize these interactions. These aperture sizes were 1.0, 1.2, 1.5, 1.8, 2.0, 2.5, and 3.0 mm.

Figure 2 illustrates the effects of masking the AOM aperture. Figure 2A again shows Cu emission with the AOM in place and the 2 × 20 mm aperture. Shown in Fig. 2B is a spectrum obtained following the placement

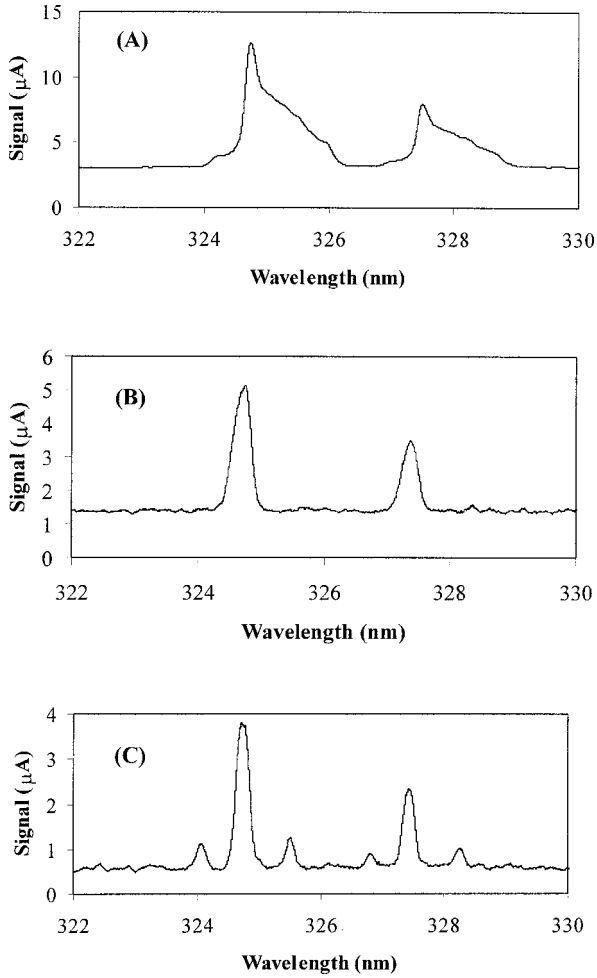

FIG. 2. Cu emission spectral effects of the AOM with a 1.5 mm circular aperture. (**A**) Original 2 × 20 mm rectangular aperture and driver power off. (**B**) 1.5 mm aperture and the AOM driver power off. (**C**) 1.5 mm aperture, AOM driver power at 5 W, and frequency of 74 MHz.

of a 1.5 mm aperture mask over the entrance of the AOM. The 1.5 mm aperture markedly decreases the observed zero-order peak widths from FWHM of 1.2 to 0.3 nm. It should be noted that application of the mask decreases the intensity of the radiation by roughly 50%. However, a more symmetrical peak shape is obtained due to the smaller amount of radiation entering the AOM at angles other than the acceptance angle of the device. As seen in Fig. 2C, with application of 74 MHz to the AO device at a driver power of 5 W, first-order AO diffraction of the 324.7 nm Cu line appears at the monochromator calibrated position of 325.4 nm. Minus-one-order diffraction appears at 324.0 nm. Similarly, first and minus-one-order 327.4 nm Cu emission are seen at 328.2 and 326.8 nm. The FWHM for the diffracted lines is 0.2 nm.

Examinations were performed to determine which mask diameter was the best compromise between radiation throughput and minimization of reflections within the AO medium. Spectra of 100 μg/mL Cu were acquired using the ICP, incorporating the various diameter apertures with the AOM operating at 74 MHz and 5 W driver power. The peak widths of zero- and first-order Cu emission were monitored versus aperture diameter. In general, the first-order peak FWHM are relatively constant. These

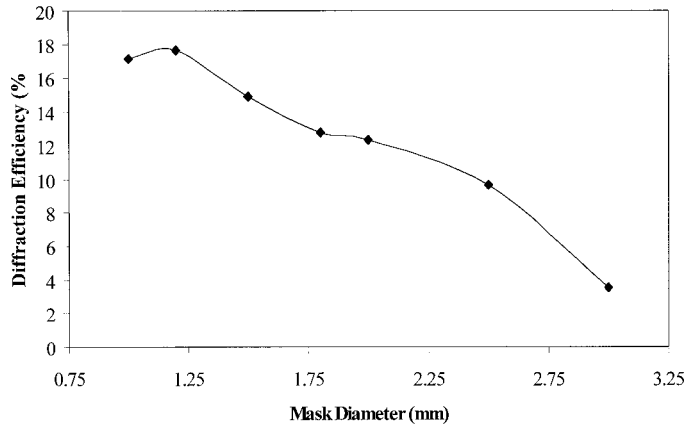

FIG. 3. 324.7 nm Cu first-order diffraction efficiency as a function of aperture size.

values ranged from 0.26 to 0.33 nm. However, the zero-order peak widths become larger with aperture diameters greater than 1.5 mm. Similar trends were observed with the glass AOD.[13] As seen with the AOD, larger apertures produced an increase in first-order diffracted peak intensity with the fused silica AOM. The relationship between first-order diffraction efficiency (peak area of first-order diffracted peak relative to the zero-order peak with the AO "off") and mask diameter is illustrated in Fig. 3. As the mask diameter is decreased, the diffraction efficiency increases. This trend is due to the reduction of radiation at angles greater than the AOM acceptance angle entering the device when the aperture is small. Based upon the compromise of the avoidance of peak broadening and the desire to maximize light throughput, the 1.5 mm aperture was selected.

Applied Acousto-Optic Frequency. Using the 1.5-mm-diameter aperture, a series of spectral scans were taken of the 324.7 nm Cu ICP emission line to develop the relationship between applied AOM driver frequency and first-order diffracted peak height. The AOM driver frequency was varied from 50 to 90 MHz in 2 MHz increments while keeping the driver power constant at 5 W. The results for these experiments are shown in Fig. 4. As can be seen from Fig. 4A, the optimum frequency for the fused silica AOM is 68 MHz based on first-order peak height. Based on diffraction efficiency and shown in Fig. 4B, the best frequency is 68 MHz. Similar to experiments noted in Ref. 13, the optimum frequency for the glass AOD was determined to be 36 MHz. This frequency yields the largest first-order peak height and the largest diffraction efficiency for 437.4 nm Sc emission with the ICP. It should be noted that those optimal frequencies will vary somewhat with different AO incident angles.

To observe background radiation, the AO driver frequency may be stepped to a second frequency. This second acoustic frequency changes the angle of the first-order peak diffraction (θ), moving the peak on the focal plane. This phenomenon is understood by examination of Eq. 1:[11,12,16]

$$\theta = \frac{\lambda F}{2v} \tag{1}$$

where λ is the optical wavelength, F is the applied acous-

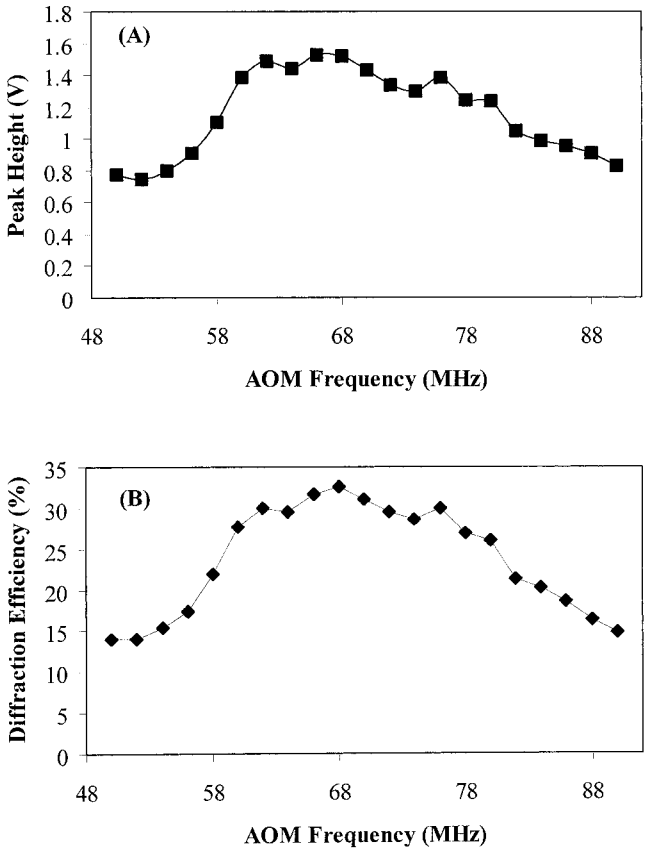

FIG. 4. First-order peak height and diffraction efficiency of 324.7 nm Cu emission with the fused silica AOM. (**A**) Peak height as a function of AOM frequency. (**B**) Diffraction efficiency as a function of AOM frequency.

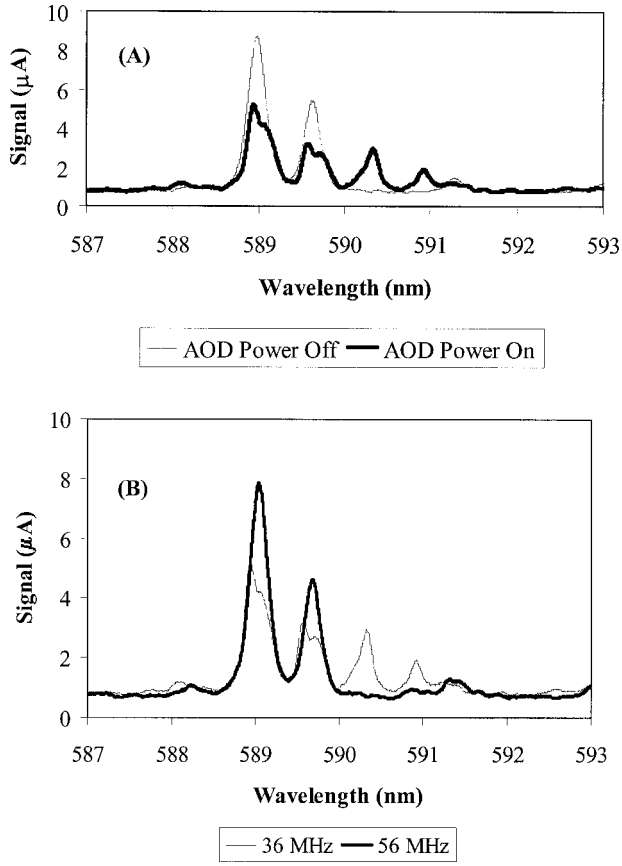

FIG. 5. Spectrum of 100 μg/mL Na with the glass AOD. Solution introduced with pneumatic nebulization. (**A**) AOD power off (thin line) and 4 W power on, 36 MHz applied frequency (heavy line). (**B**) AOD power on at 4 W and applied frequencies of 36 MHz (thin line) and 54 MHz (heavy line).

tic frequency, and v is the velocity of the acoustic waves within the AO medium. Since v is constant for the AO materials, an increase in F will increase the angle of AO diffraction. If a first-order deflection peak is monitored by the PMT, the peak can be shifted on and off of the exit slit by varying F. By modulating the frequency applied to the AO device, the analytical signal and background signal can alternately be monitored. The background-corrected analytical signal can then be calculated by subtracting the background "off-line" signal from the analytical "on-line" signal. Since a variety of background peaks are present from the argon ICP gas, the required deflection to monitor the background under a first-order peak varies with the element and wavelength to be monitored.

To determine the appropriate frequency for adequate background signal measurement, spectral scans were taken for each of the elements while applying varying frequencies to the AO device. As an example, Fig. 5 shows the optimized applied frequencies for background measurements of Na with the glass AO device. In Fig. 5A, the thin line represents the Na spectrum with the AOD driver power off. Only zero-order peaks are seen for Na at 588.995 and 589.592 nm. An argon 588.859 nm background line overlaps the 588.995 nm Na line. The heavy line in this figure represents the spectrum when the AOD driver is operated at 4 W and 36 MHz. The first-order deflected 588.995 nm Na line appears at 590.4 nm and the first-order 589.592 nm Na line appears at 590.8 nm. For background correction of the two Na emission peaks, the AOD frequency is modulated. In Fig. 5B, spectra taken with two applied frequencies are shown. By setting the monochromator to 590.4 nm, the signal is on-line (measuring the analytical signal) with the frequency set at 36 MHz and off-line (measuring the background signal) at 54 MHz. At 54 MHz, this peak is deflected to a higher monochromator calibrated wavelength (590.7 nm). Therefore, the background signal is measured when the monochromator wavelength is held constant at 590.4 nm. By modulating the frequency applied to the AO from 36 MHz to 54 MHz, analytical signal and background are sequentially measured and the background-corrected signal can be calculated. It should be noted that the Ar peak at 588.859 nm is also deflected into an AO first-order peak. This peak is underneath the AO first-order 588.995 nm Na peak. Therefore, when modulating, the Ar peak is always present with the Na peak, contributing additional background noise.

With the fused silica AOM, similar optimization studies were performed with all elements with emission peaks from 200 to 400 nm. As an example, spectra of 328.068 nm Ag emission are shown in Fig. 6A. With the driver frequency set at 68 MHz, the first-order Ag peak appears at 328.8 nm and the negative first-order peak can be seen at 327.3 nm. When the AOM is operated at 68 MHz and

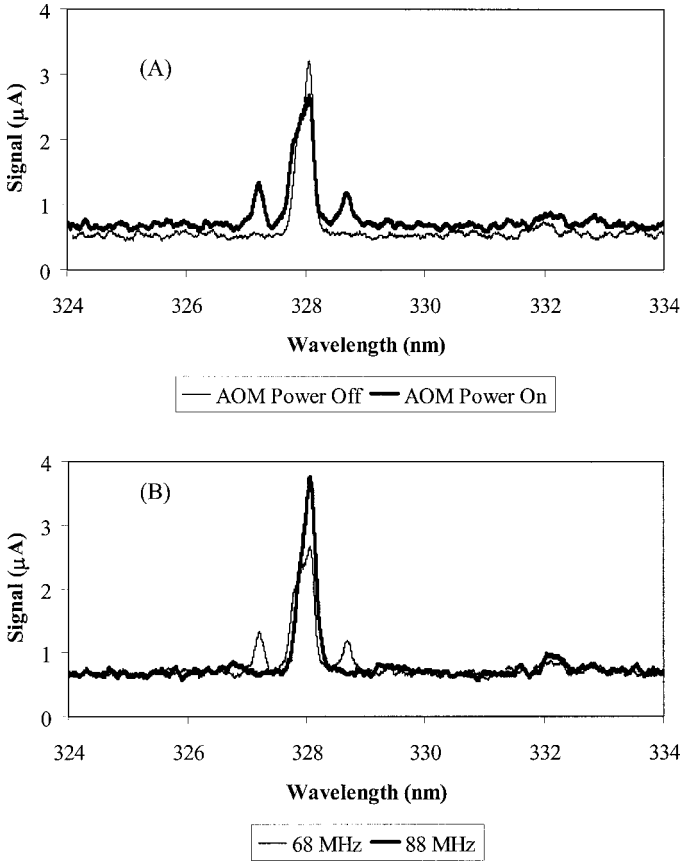

FIG. 6. Spectrum of 100 μg/mL Ag with the fused silica AOM. Solutions introduced with pneumatic nebulization. (**A**) AOM power off (thin line) and 5 W power, 68 MHz applied frequency (heavy line). (**B**) AOM power on at 5 W and applied frequencies of 68 MHz (thin line) and 88 MHz (heavy line).

the monochromator is set for first-order emission to be detected by the PMT (328.8 nm), the analytical Ag signal can be measured. With the AO frequency at 88 MHz, the first-order Ag peak is deflected to the monochromator calibrated position of 329.2 nm. Therefore, when set for 68 MHz first-order Ag at 328.8 nm on the monochromator, changing the frequency to 88 MHz allows measurement of the background signal. The results of these studies for all elements analyzed with the glass and fused silica AOs are shown in Table II.

Pneumatic Nebulization. Calibration plots were generated for all elements using pneumatic nebulization and the appropriate ''on-line'' and ''off-line'' AO frequencies. The first-order peak was directed to the exit slit and the monochromator wavelength setting was kept constant throughout the determination. A 150 Hz background correction AO modulation rate with a data acquisition rate of 40 kHz and 2 s data acquisition time were applied. Twenty data points were taken per half cycle of the modulation. To this data a 20-point boxcar average was employed to smooth each data set. Therefore, one data point is calculated for ''off-line'' and ''on-line'' conditions for each cycle of the modulation. The linear ranges for these analyses are shown in Table III. For pneumatic nebulization studies, linearity was good, with r^2 values ranging from 0.997 to 0.9999991.

Electrothermal Vaporization. Electrothermal vaporization conditions were optimized for each element analyzed. For each determination, 15 μL samples were injected into the carbon cup and, if needed, 5 μL of $Mg(NO_3)_2$ matrix modifier. Elements that required matrix modification were Ba, Be, Co, Cr, Fe, and Zn. In general, solvent dry times varied from 15 to 60 s. The atomization step conditions varied from element to element and the times ranged from 1.5 to 3.0 s. Calibration plots were constructed and the linear concentration ranges for each element are shown in Table III. A 400-point box car average (0.25 s) was used to smooth the data collected. To accomplish this, 400 cycles of the 20 raw data points/cycle set were averaged to produce a single data point. As an example, Fig. 7 shows the background-corrected signal versus time profiles for several elements at a 100 μg/mL concentration. As can be seen from this figure, Eu, Co, Fe, Cr (267 nm), Ag, and Cu all yield symmetrical peaks at the optimum conditions with varying sensitivity. With ETV sample introduction, linearity was also good, with r^2 values ranging from 0.991 to 0.999997.

TABLE III. Varian Liberty Series II axial ICP-AES operating conditions.[a]

Element	Wavelength (nm)	Range of standard concentrations: Pneumatic (μg/mL)	Range of standard concentrations: ETV (ng)	r^2 values: Pneumatic	r^2 values: ETV
Ag[b]	328.068 I	5–100	15–570	0.9995	0.9998
Ba[b]	233.527 II	5–100	75–1500	0.9991	0.999990
Be[b]	234.861 I	5–100	60–1500	0.9997	0.99990
Ca[b]	393.366 II	0.1–50	1.5–150	0.9995	0.997
Ca[c]	422.673 I	3–100	45–1500	0.997	0.997
Cd[b]	214.438 II	5–100	75–1500	0.9992	0.999997
Co[b]	228.616 II	5–100	75–1500	0.99995	0.9996
Cr[b]	267.716 II	5–100	15–1500	0.99992	0.997
Cr[c]	427.291 I	20–100	75–270	0.999993	0.991
Cr[c]	428.972 I	10–100	75–675	0.997	0.991
Cu[b]	324.754 I	5–100	15–300	0.99995	0.9990
Eu[b]	381.967 II	5–100	60–775	0.9997	0.9993
Fe[b]	238.204 II	5–100	75–1500	0.9995	0.9998
Li[c]	670.776 I	10–100	150–1500	0.9999991	0.992
Mg[b]	280.270 II	5–100	75–1500	0.9991	0.9994
Mn[b]	257.610 II	1–100	15–1500	0.9991	0.98
Mn[c]	403.076 I	20–100	15–1500	0.99997	0.99997
Na[c]	588.995 I	10–100	15–1500	0.99998	0.990
Na[c]	589.592 I	25–100	15–375	0.997	0.998
Pb[b]	220.353 II	20–150	150–2250	0.99990	0.9998
Sc[b]	361.384 II	2–100	150–750	0.9993	0.99998
Sc[c]	437.446 II	2–30	300–750	0.9993	0.998
Zn[b]	213.856 I	10–100	75–750	0.997	0.992

[a] RF power: 1.2 kW, auxiliary Ar flow: 1.5 L/min, coolant Ar flow: 15 L/min with pneumatic nebulization, 18 L/min with ETV, nebulizer pressure: 100 kPa, pump speed: 2.0 mL/min.
[b] Determined with the fused silica AOM.
[c] Determined with the flint glass AOD.

Detection Limits. Table IV lists the detection limits calculated for each element with pneumatic and ETV sample introduction using acousto-optic deflector background correction. The detection limit was calculated as the mass or concentration that yielded a signal three times the standard deviation of the blank divided by the slope of the calibration plot. Twenty-three detection limits were calculated from data obtained using either the glass or fused silica AO background correction systems. Pneumatic nebulization detection limits ranged from 0.3 μg/mL for Be and Fe to 20 μg/mL for Na at 589.592 nm. Electrothermal vaporization detection limits ranged from

TABLE IV. Detection limits.

Element	Wavelength (nm)	Pneumatic detection limit (μg/mL)	ETV detection limit[a] (ng)
Ag	328.068	3	11
Ba[b]	233.527	0.9	60
Be[b]	234.861	0.3	44
Ca	393.366	0.8	9
Ca	422.673	3	8
Cd	214.438	2	16
Co[b]	228.616	2	17
Cr[b]	267.716	4	15
Cr	427.291	5	34
Cr	428.972	6	19
Cu	324.754	1	6
Eu	381.967	1	1
Fe[b]	238.204	0.3	65
Li	670.776	6	100
Mg	280.270	0.4	16
Mn	257.610	0.5	3
Mn	403.076	9	11
Na	588.995	5	5
Na	589.592	20	3
Pb	220.353	8	8
Sc	361.384	1	3
Sc	437.446	2	5
Zn[b]	213.856	5	17

[a] Sample size is 15 μL and signal monitored is peak height.
[b] 50 mg of $Mg(NO_3)_2$ modifier added to each sample.

1 ng (Eu) to 100 ng (Li). The detection limits were higher than we hoped, due to a noisy blank signal. Since the standard deviations of the blank signals were large, the detection limits calculated were worse than we expected.

Water and Vitamin Samples. To examine the applicability of the system to real samples, water and vitamin tablets were prepared using pneumatic nebulization ICP-AES and FAA analysis. Flame AA was performed to compare the validity of the values obtained with our background correction system. Calibration plots were constructed for Ca, Cu, Fe, Mg, Mn, and Zn with each technique. Table V lists the results of the analysis of the water samples and vitamin tablets by ICP and FAA. Because the Cu, Fe, and Mn concentrations in water were low, valid comparative results could not be obtained. Overall, the ICP and FAA methods yield similar mean concentrations for both the water samples and the vitamin samples. The fused silica AOM results agree with the label value for each element in the vitamin tablet with an

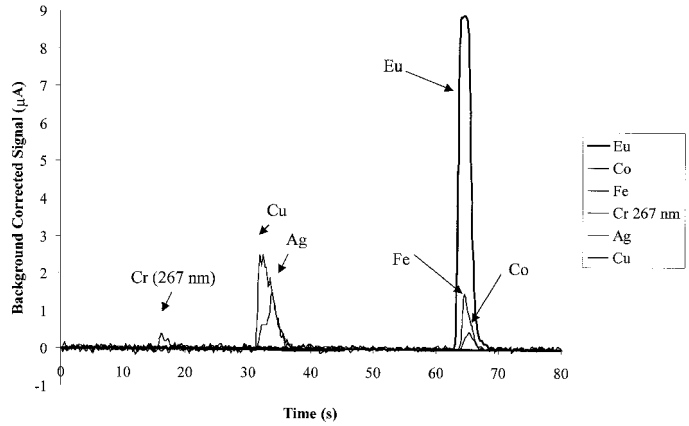

FIG. 7. Electrothermal vaporization sample introduction emission profiles of aqueous 100 μg/mL solutions of Eu, Co, Fe, Cr (267.7 nm), Ag, and Cu using the fused silica AOM.

average absolute difference of 15%. The FAA results have 14% average absolute difference with the label value of the tablet. Therefore, our background correction system is comparable to FAA. The glass AOD had an average percent difference of ±6% when compared to the label value of the vitamin samples. When comparing the mean concentrations for AO-ICP and FAA in the water samples, the average absolute differences between the two techniques is 11% for Ca, 17% for Mg, and 26% for Zn. It is likely the large error for Zn arises due to the statistical fluctuation of being near the 5 μg/mL Zn detection limit with the AO-ICP system. In general, these results show promise for future development and usage of AOD background correction for trace-metal analysis with ICP-AES.

CONCLUSION

Acousto-optic deflector and modulator background correction was successfully characterized with ICP-AES. The fused silica AOM and glass AOD allowed background correction to be performed in the spectral range of 200 to 700 nm. Linear ranges and detection limits were established. Since the detection limits obtained were not as good as were expected, alternative data analysis techniques will be explored. To decrease the noise in the signals, smoothing techniques and power spectral analysis

TABLE V. Real-world sample results.

		Concentration (μg/mL)[a]				Percent difference (%)[d]		
	Element	ICP-fused silica AOM	ICP-glass AOD	FAA	Label value (μg/mL)	ICP-fused silica AOM	ICP-glass AOD	FAA
Vitamin samples	Ca	1500 ± 200	1600 ± 200	1400 ± 200	1620	−8	−1	−14
	Cu	26 ± 8	—[b]	16 ± 6	20	+30	—[b]	−20
	Fe	200 ± 60	—[b]	180 ± 60	180	+11	—[b]	0
	Mg	960 ± 180	—[b]	900 ± 160	1000	−4.0	—[b]	−10
	Mn	22 ± 3	18 ± 7	—[c]	20	+10	−10	—[c]
	Zn	110 ± 30	—[b]	170 ± 20	150	−27	—[b]	+13
Water samples	Ca	100 ± 1	80 ± 4	92.7 ± 0.5				
	Mg	39 ± 3	—[b]	47.1 ± 2.8				
	Zn	2.5 ± 0.5	—[b]	3.4 ± 0.1				

[a] Values reported are the average of 5 different samples ± standard deviation of the 5 samples.
[b] Not determined due to lack of emission line in wavelength region.
[c] Not determined due to lack of Mn HCL.
[d] Compared to label value.

will be performed. Metals analysis of real-world samples has been performed with our system. Tap water and vitamin tablet samples were analyzed quickly and accurately. These results show promise for analysis of other types of samples with our AOD background correction with ICP-AES.

1. M. A. Saleh, E. Ewane, J. Jones, and B. L. Wilson, J. Food Comp. Anal. **14,** 127 (2001).
2. N. J. Miller-Ihli, J. Agric. Food Chem. **44,** 2675 (1996).
3. P. Mattila, K. Konko, M. Eurola, J.-M. Pihlava, J. Astola, L. Vahteristo, V. Hietaniemi, J. Kumpulainen, M. Valtonen, and V. Piironen, J. Agric. Food Chem. **49,** 2343 (2001).
4. P. L. Fernandez-Caceres, M. J. Martin, F. Pablos, and A. G. Gonzalez, J. Agric. Food Chem. **49,** 4775 (2001).
5. H. L. Peters, K. E. Levine, and B. T. Jones, Anal. Chem. **73,** 453 (2001).
6. S. M. Pyle, J. M. Nocerino, S. N. Deming, J. A. Palasota, J. M. Palasota, E. L. Miller, D. C. Hillman, C. A. Kuharic, W. H. Cole, P. M. Fitzpatrick, M. A. Watson, and K. D. Nichols, Environ. Sci. Technol. **30,** 204 (1996).
7. J. Dombovari and L. Papp, Microchem. J. **59,** 187 (1998).
8. O. Vicente, A. Masi, L. Martinez, R. Olsina, and E. Marchevsky, Anal. Chim. Acta **366,** 201 (1998).
9. J. A. Deblaquiere, K. C. Harvery, and A. K. Hellman, Am. J. Phys. **59,** 443 (1991).
10. C. D. Tran, Anal. Chem. **64,** 971A (1991).
11. R. V. Johnson, ''Design of Acousto-Optic Modulators'', in *Design and Fabrication of Acousto-Optic Devices*, A. P. Goutzoulis and D. R. Pape, Eds. (Marcel Dekker, New York, 1994), Chap. 3, p. 123.
12. D. R. Pape, O. B. Gusev, S. V. Kulakov, and V. V. Molotok, ''Design of Acousto-Optic Deflectors'', in *Design and Fabrication of Acousto-Optic Devices*, A. P. Goutzoulis and D. R. Pape, Eds. (Marcel Dekker, New York, 1994), Chap. 2, p. 69.
13. T. M. Spudich and J. W. Carnahan, J. Anal. At. Spectrom. **16,** 56 (2001).
14. U. Schaffer and V. Krivan, Anal. Chem. **70,** 482 (1998).
15. M. Wu and J. W. Carnahan, Appl. Spectrosc. **44,** 673 (1990).
16. T. M. Spudich, B. A. Pelz, and J. W. Carnahan, Appl. Spectrosc. **51,** 765 (1997).